Influence of the Configuration of the Magnetic Filter Field on the Discharge Structure in the RF Driven Negative Ion Source Prototype for Fusion

S. Lishev[1, a)], L. Schiesko,[2] D. Wünderlich[2] and U. Fantz[2]

[1]*Faculty of Physics, Sofia University, 5 J. Bourchier Blvd., BG-1164 Sofia, Bulgaria*
[2]*Max-Planck-Institut für Plasmaphysik, Boltzmannstr. 2, 85748 Garching, Germany.*

[a)]lishev@phys.uni-sofia.bg

Abstract. The study provides results of the influence of the filter field topology on the plasma parameters in the RF prototype negative ion source for ITER. A previously developed 2D fluid plasma model has been extended to take into account for the particles and energy losses along the magnetic field lines and the presence of a magnetic field in the driver as it is the case for the BATMAN and ELISE test-beds. Since the main role of the magnetic filters in these two sources is the same (to reduce the co-extracted electron current) they are studied and compared for the geometry of the prototype source. For the magnetic field configuration used at BATMAN, the axial position of the filter has been varied according to experiments with an external magnet frame. For the magnetic field configuration of ELISE the magnitude of the field has been varied, as can be done in the experiment by varying the current flowing through the first grid of the extraction system. The obtained results show the same main features in the patterns of the plasma parameters for the two configurations of the magnetic filter. The presence of a magnetic filter in the driver has a local impact on the plasma parameters, showing no significant influence on their spatial distributions in the expansion chamber.

INTRODUCTION

The magnetic filters are one of the key components in the negative hydrogen ion sources [1,2] developed towards the neutral beam injection systems (NBI) of ITER and beyond it (i.e., for DEMO). In a view of performance of the sources, the main role of the magnetic filter (MF) is to reduce, both, the electron temperature and the current of the co-extracted electrons by means of a transverse magnetic field. However, the magnetic field introduces significant modifications in the spatial structure of the plasma parameters [3-9].

The fluid models on the operation of the MF [5] have shown that the effect of electron cooling is due to suppressed thermal conductivity caused by the filter field (FF). Diffusion (suppressed by the FF) and thermal diffusion (gained by the drop of the electron temperature) acting in a combination are in basis of the formation of a maximum of the electron density in the region of the MF. Further on, thermal fluxes related to the diamagnetic drift (carrying energy behind the MF) causes formation of a groove in the spatial distribution of the electron temperature (a region with low values) and the (E×B)-drift shifts out-of-the center the maximum of the electron density.

The RF driven negative ion source prototype (1/8 of the ITER source [10]) is an inductively driven tandem type source based on surface production of the ions with a cylindrical driver and a rectangular expansion chamber. The MF configuration of the BATMAN test facility is formed by internal magnets (embedded into the diagnostic flange) or by an axially movable magnet frame attached to the expansion chamber [1]. The ELISE source (1/2 of the ITER source [2] is also an inductively driven tandem type source based on surface production of the ions, but with four cylindrical drivers attached to a rectangular expansion chamber (~1×1 m^2). The MF configuration in ELISE is produced by a current flowing though the plasma grid (PG), a feature, which is planned to be investigated also at the prototype source [11]. The topology of the MF in these two sources is quite different, but a common point is that the FF is present everywhere in the source volume (including its driver).

The ITER relevant negative ion sources (like BATMAM and ELISE) are the basis for further optimizations towards the NBI systems for DEMO. The modelling of these sources – providing results for the plasma parameters at varying conditions – is a valuable tool. In this direction, the fluid-plasma-models have an advantage, since they can be easily applied in the overall description of the fusion-sources and, thus, used at their improvement.

Studying different type of the MF (i.e., the configuration of the MF of ELISE) as well as taking into account for the presence of a magnetic field in the driver are issues not addressed yet in the models applied for the RF prototype source [6-8]. Accounting for the charged particle and energy losses along the magnetic field lines is another issue, starting to be considered in the PIC-codes, but not taken into account in the 2D–fluid–models. Although it does not introduce qualitative changes in the pattern of the plasma parameters [5], the fluxes along the FF could reduce significantly the fluxes in the transverse direction, where the 2D models are applied. Involving the complicated geometry of the prototype source without accounting for the FF in the driver [6-8] shows the known [5] pattern of the plasma parameters. However, in the previous model [8] it was identified that effects of the plasma expansion into the bigger volume of the second chamber are superimposed on the effects of plasma expansion through the MF as well as shifting the entire discharge pattern in correlation with the shift of the position of the filter.

FORMULATION OF THE PROBLEM AND SET OF EQUATIONS

The aim of the study is to investigate the influence of the magnetic field topology of BATMAN and ELISE on the plasma parameters in the geometry of the RF prototype negative ion source for ITER.

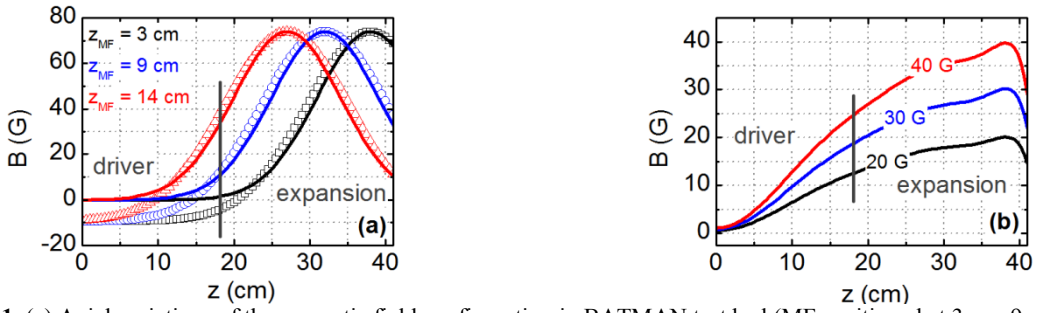

FIGURE 1. (a) Axial variations of the magnetic field configuration in BATMAN test bed (MF positioned at 3 cm, 9 cm and 14 cm from the plasma grid): with account for the FF inside the driver (symbols) and without FF in the driver (solid lines). (b) Axial variations of the magnetic field produced by a current flowing into the plasma grid (ELISE-like).

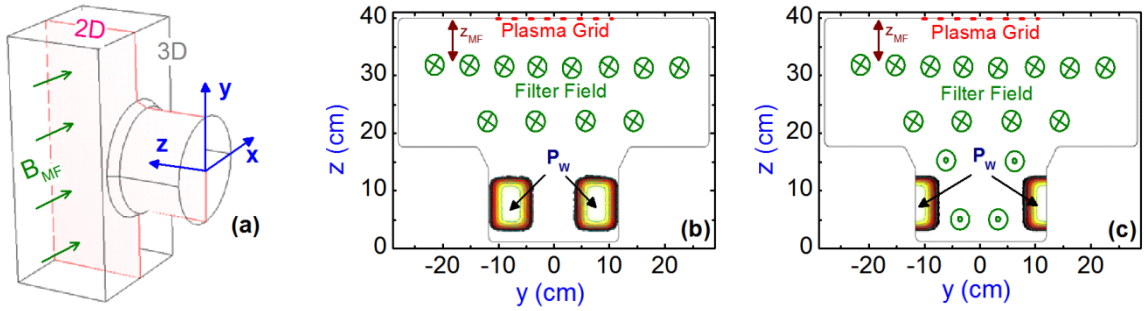

FIGURE 2. Modeling domains in the 3D geometry (a) and in the 2D planar geometry (in the (*z*-*y*)-plane, transverse to the magnetic field) with: (b) wide region of RF power deposition and (c) localized RF power deposition at the walls of the driver.

The magnetic field configurations of BATMAN are like in the experiments [1,4] (shown with symbols in Fig. 1(a)). The axial position of maximum value of the magnetic field in the expansion region (74 G) fixes the three positions of the filter – z_{MF} = 3 cm (the standard configuration with internal magnets), 9 cm and 14 cm (with magnet frame), from the plasma grid – and, thus, determines the configuration of the magnetic field. The FF in the driver is in the opposite direction (with respect to the expansion region) and its maximum value of – 9.4 G is at the bottom of the driver. In order to identify the influence of the magnetic filter on the plasma parameters, a comparison is made between the configurations with and without FF inside the driver as shown in Fig. 1(a). The magnetic field in the ELISE source is produced by a current flowing though the plasma grid [2]. As it is shown in Fig. 1(b), the magnetic

field of the ELISE, considered here, have wider profile than the magnetic field configurations of BATMAN, with maximum value at a fixed position just in front of the plasma grid. In order to reduce the computational effort the configuration of the MF of ELISE is studied at the geometry of the prototype source, varying the strength of the magnetic field induction from 20 G up to 40 G (Fig. 1(b)). The magnetic field in the vicinity of the PG is overlapped with the deflection magnetic field (produced by the magnets embedded in the extraction grid). However, since the extraction physics is not in the focus of this study, the latter is not taken into account.

A proper approach of the complicated 3D geometry of the RF prototype source (presented schematically in Fig. 2(a)) is a 2D planar geometry description in the (*y*-*z*)-plane which is perpendicular to the direction of the magnetic field lines (Fig. 2(b)) [8]. However, due to the finite scales of the driver and the expansion plasma volume in the third *x*-direction, the losses of particles and energy along it may also plays a role in the formation of the discharge structure. In the presence of a magnetic field in the driver, there is no expanding plasma region between the RF power deposition and the expansion chamber of the source, which means a strong increase of the locality in the driver. Therefore, the previously developed 2D fluid plasma model for a hydrogen discharge in a free-fall regime [8] is extended towards accounting for the losses due to the third dimension and the presence of a magnetic field in the driver. Regarding the latter issue, the region of the RF power deposition (Fig. 1(b)) is shifted towards the walls of the driver (Fig. 1(c)). The former issue is estimated by introducing of an additional loss terms (L_α, L_N and L_J) in the initial set of equations of the 2D model (the continuity equations of the electrons (α = e) and the three types of positive ions ($\alpha \equiv j$ = 1, 2, 3 for H^+, H_2^+ and H_3^+ ions), the continuity equation for the hydrogen atoms, the electron energy balance equation and the Poisson equation):

$$\mathrm{div}_{(y,z)}\,\boldsymbol{\Gamma}_\alpha = (\delta n_\alpha / \delta t) - L_\alpha \tag{1}$$

$$\mathrm{div}_{(y,z)}(-D_\mathrm{a}\nabla N_\mathrm{a}) = (\delta N_\mathrm{a} / \delta t) - L_\mathrm{N} \tag{2}$$

$$\mathrm{div}_{(y,z)}\,\mathbf{J}_\mathrm{e} = P_\mathrm{ext} + P_\mathrm{coll} - e\boldsymbol{\Gamma}_\mathrm{e}\cdot\mathbf{E}_\mathrm{dc} - L_\mathrm{T} \tag{3}$$

$$\Delta\Phi = -\frac{e}{\varepsilon_0}\left(\sum_{j=1}^{3} n_j - n_\mathrm{e}\right). \tag{4}$$

In Eq. (1-4) n_α are the densities of the charged particles and $\boldsymbol{\Gamma}_\alpha$ are their fluxes, D_a is the diffusion coefficient of the hydrogen atoms, $\mathbf{J}_\mathrm{e}$ is the electron energy flux, Φ is the potential of the dc electric field in the discharge ($\mathbf{E}_\mathrm{dc}$ = - grad Φ); e and ε_0 are, respectively, the elementary charge and the vacuum permittivity. The density of the hydrogen molecules N_m is determined through the equation of state $p = \kappa T_\mathrm{g}(N_\mathrm{a}+N_\mathrm{m})$, where κ is the Boltzmann constant, T_g is the gas temperature and N_a is the densities of the hydrogen atoms.

The electrons are the only magnetized charged particles and, thus, their (particle and energy) fluxes in the (*y*-*z*)-plane are affected by the magnetic field. The *y*- and *z*- components of the electron flux $\boldsymbol{\Gamma}_\mathrm{e}$ account for: electron mobility, diffusion and thermal diffusion across the magnetic field, the $\mathbf{E}\times\mathbf{B}$ drift and the diamagnetic drifts due to density and electron temperature (T_e) gradients. The *y*- and *z*- components of the electron energy flux $\mathbf{J}_\mathrm{e}$ involve the thermal flux across the magnetic field, the thermal flux related to the diamagnetic drift (both forming the conductive energy flux) and the convective energy flux.

The first assumption in the estimation of the additional losses is for conservation of the fluxes in the *x*-direction (i.e., virtually from the (*y*-*z*)-plane till the side-walls of the driver and the second chamber). As a result, the particles and energy losses via fluxes in the third direction ($\Gamma_\alpha(x)$ and $J_\mathrm{e}(x)$ in their drift-diffusion form) can be given by the standard expressions for the boundary conditions. The second assumption is for the scaling of these fluxes as $\partial_x \approx 1/R_{(\mathrm{D,\,E})}$, where $R_{(\mathrm{D,\,E})}$ denote the characteristic size of the driver ($2R_\mathrm{D}$ = 24.4 cm) and of the second chamber ($2R_\mathrm{E}$ = 30.9 cm). The third assumption is for Boltzmann distribution of the electron density in the *x*-direction: $n_\mathrm{e} = n_{e0}\exp(-\Phi/T_\mathrm{e})$. Thus, the last terms in the right-hand sides of (1-4) takes the form:

$$L_\mathrm{e}(y,z) = R_{(\mathrm{D,\,E})}^{-1}\left(0.25\upsilon_{\mathrm{th,e}}\, n_\mathrm{e}\right) \tag{5a}$$

$$L_j(y,z) = R_{(\mathrm{D,\,E})}^{-1}\left(b_j^{\mathrm{eff}}\, n_j\Phi + 0.5\upsilon_{\mathrm{th},j}\, n_j\right) \tag{5b}$$

$$L_\mathrm{T}(y,z) = R_{(\mathrm{D,\,E})}^{-1}\left[\left(5/2eT_\mathrm{e}\right)\left(0.25\upsilon_{\mathrm{th,e}}\, n_\mathrm{e}\right) + e\left(R_{(\mathrm{D,\,E})}^{-1}\Phi\right)\left(0.25\upsilon_{\mathrm{th,e}}\, n_\mathrm{e}\right)\right] \tag{5c}$$

$$L_\mathrm{N}(y,z) = R_{(\mathrm{D,E})}^{-1}\left(0.25\gamma\upsilon_{\mathrm{th,a}}\, N_\mathrm{a}\right). \tag{5d}$$

In (5) υ_th is the thermal velocity of a given particle species, b_j^{eff} is the effective mobility of the positive ions (specifying the free-fall regime [12]) and γ is the recombination efficiency of the hydrogen atoms at the walls. The last term in (5c) is the electron energy loss for sustaining the dc electric field in the *x*-direction.

RESULTS AND DISCUSSIONS

The results here are obtained for the configuration and operational conditions of the prototype RF source as in Ref. [4, 8]: absorbed RF power of 40 kW and gas pressure $p = 0.6$ Pa. Here, the bias of the PG is fixed at $U_{PG} = 10$ V with respect to the grounded walls of the source. The RF power deposition is externally applied and it has a supper-Gaussian profile in y- and z-direction.

Evaluation of the Consistency of the Losses Due to the Third Dimension

In order to verify the simplified manner of accounting for the losses along the x-axis, results for the plasma parameters obtained from the 2D model, with and without expressions (5) involved in the initial system (1-4), are compared with results from a 3D model [8]. The results are obtained without a MF and without a bias applied to the PG. Also, the gas pressure is higher (1.6 Pa).

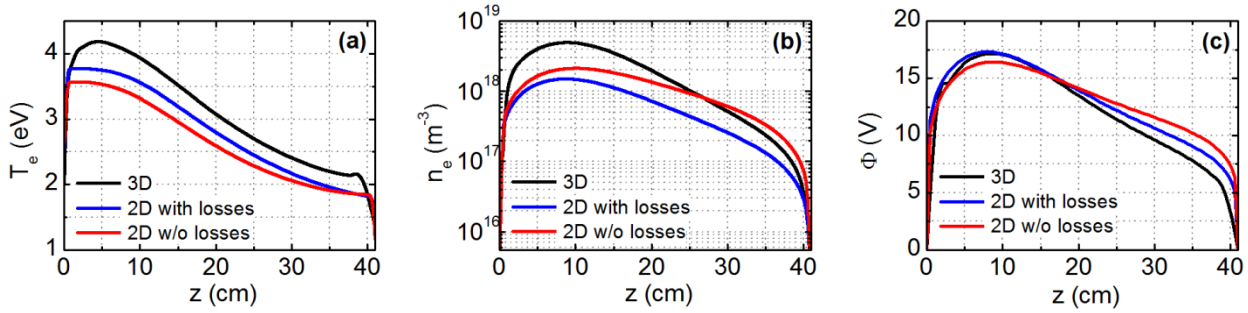

FIGURE 3. Axial variations of the electron temperature (a), of the electron density (b) and of the plasma potential (c) obtained within the 3D- and 2D-models without MF at $U_{PG} = 0$; gas pressure of 1.6 Pa and absorbed power 40 kW (with a wide region of RF power deposition).

As it could be expected, accounting for the additional losses in the 2D model lead to higher electron temperature (Fig. 3(a)) and lower electron density (Fig. 3(b)). Compared with the results from the 3D model, the two 2D models (with and without accounting for the additional loses) shows a partial match. However, the axial profiles of the electron temperature (Fig. 3(a)) and plasma potential (Fig. 3(c)) obtained from the 2D model with account for the losses are closer to the corresponding result from the 3D model. The same concerns the axial gradients, including that of the electron density as it could be seen in Fig. 3(b). Therefore, involving the losses in the 2D model (in the simplified manner assumed here) could be considered as a reasonable approximation of the 3D case.

Influence of the Additional Losses and the RF Power Deposition Region

For the identification of the effect of the additional losses in the presence of a MF the standard configuration of the MF ($z_{MF} = 3$ cm) is considered, however, at a grounded plasma grid and without accounting for the FF in the driver. The gas pressure is 0.6 Pa, as in the experiment [4].

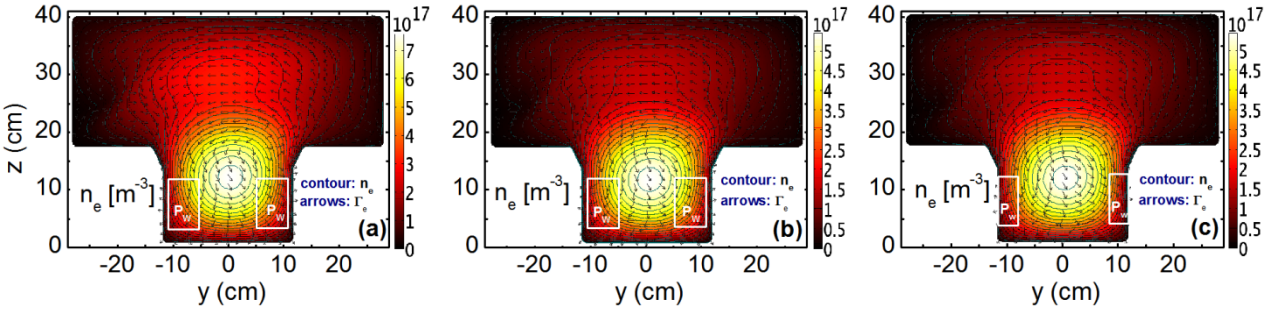

FIGURE 4. Spatial distribution of the electron density: (a) without and (b) with account for the losses along the magnetic field and (c) with RF power deposition at the walls of the driver. The MF is at $z_{MF} = 3$ cm, $P_W = 40$ kW; $p = 0.6$ Pa and $U_{PG} = 0$ V.

Without having the losses introduced (Fig. 4(a)), the electron density is with its typical pattern in an external magnetic field: a main maximum in the driver and a slightly indicated second one in the expansion chamber. Involving the losses (Fig. 3(b)) does not introduce changes in the pattern of the electron density. However, the maximum of the electron density located in the expansion chamber is less pronounced due to the suppression of the drifts by the additional fluxes along the magnetic field lines. Since the total losses are increased, the values of the electron density are lower.

The comparison of Fig. 4(c) with Fig. 4(b) shows that shifting of the RF power deposition to the walls of the driver does not introduce changes in the spatial distribution of the electron density. This is expected since, without the FF in the driver, there is enough room for the non-local processes (thermal conductivity and electron diffusion) to suppress the effect of the localized power deposition, but it will not be case when the driver becomes magnetized.

Magnetic Field Configuration of the BATMAN Test Bed

The results presented here are obtained for the magnetic field configurations of the RF prototype source used in the experiment [4]. As it is shown in Fig. 1(a), for all three positions of the filter (z_{MF} = 3 cm, 9 cm and 14 cm) the magnetic field is present not only in the second chamber of the source, but also in the driver. However, to identify the influence of the FF in the driver on the plasma parameters, first are given results without magnetic field in the driver (Figs. 5 and 6). The plasma grid is biased at U_{PG} = 10 V, the RF power deposition is localized at the walls of the driver and the losses along the magnetic field are introduced.

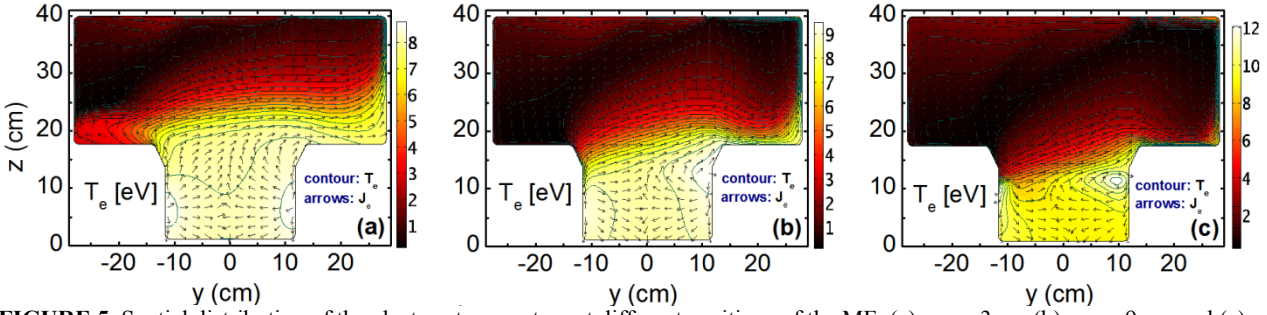

FIGURE 5. Spatial distribution of the electron temperature at different positions of the MF: (a) z_{MF} = 3 cm (b) z_{MF} = 9 cm and (c) z_{MF} = 14 cm. The results are obtained without the FF in the driver. The absorbed power is 40 kW; p = 0.6 Pa and U_{PG} = 10 V.

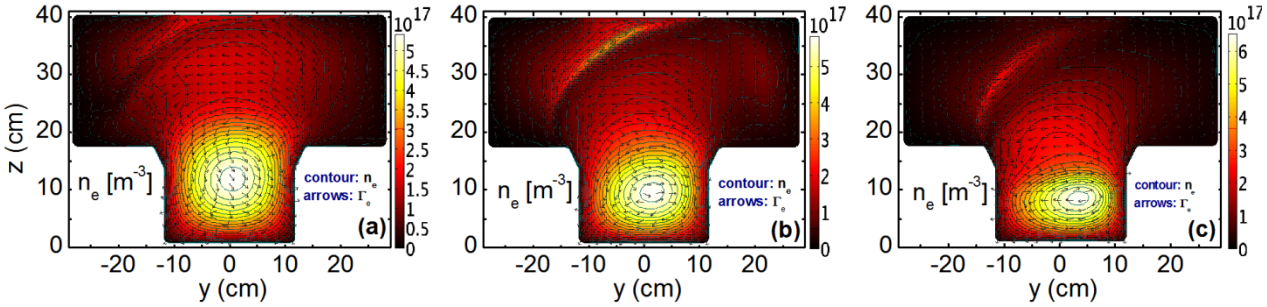

FIGURE 6. The same as in Fig. 5, but for the electron density

In accordance with the previous study [8], the presence of a magnetic field in the expansion chamber of the source leads to formation of a groove in the spatial distribution of the electron temperature along the y-axis (i.e., the region with low electron temperature in Fig. 5). However, due to the reduced electron energy fluxes when the losses along the magnetic are involved, the groove here is wider. In the absence of magnetic field in the driver, due to the high thermal conductivity there, the electron temperature has an almost flat profile. As it is shown in Figs. 5(a)-5(c) the entire pattern of the electron temperature shifts in a correlation with the position of the magnetic filter (i.e., from the plasma grid towards the driver).

The spatial distribution of the electron density (Fig. 6) is also in accordance with the previously obtained results [8], showing a main maximum in the driver and two maxima in the second chamber as well as strong accumulation of electrons in front of the plasma grid when it is biased (Fig. 4(c) compared with Fig. 6(a)). Involving the losses

along the magnetic field does not change the pattern of the electron density, for all of the positions of the magnetic filter considered, but the maxima of the electron density in the expansion region are less pronounced. The latter is due to the damping of the fluxes, forming the two maxima of the electron density, by the losses along the magnetic field. As a general trend, the entire pattern of the electron density shifts according to the position of the MF.

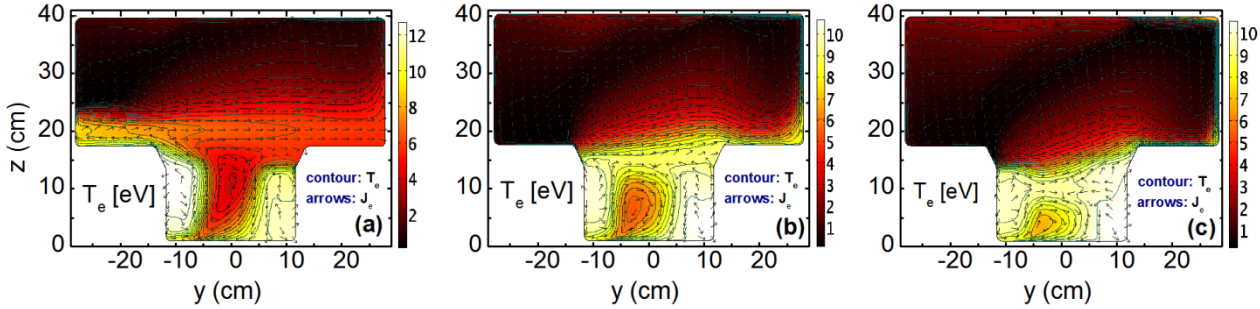

FIGURE 7. Spatial distribution of the electron temperature at different positions of the MF: (a) z_{MF} = 3 cm (b) z_{MF} = 9 cm and (c) z_{MF} = 14 cm. The results are obtained with account for the FF in the driver. The same conditions as in Fig. 5.

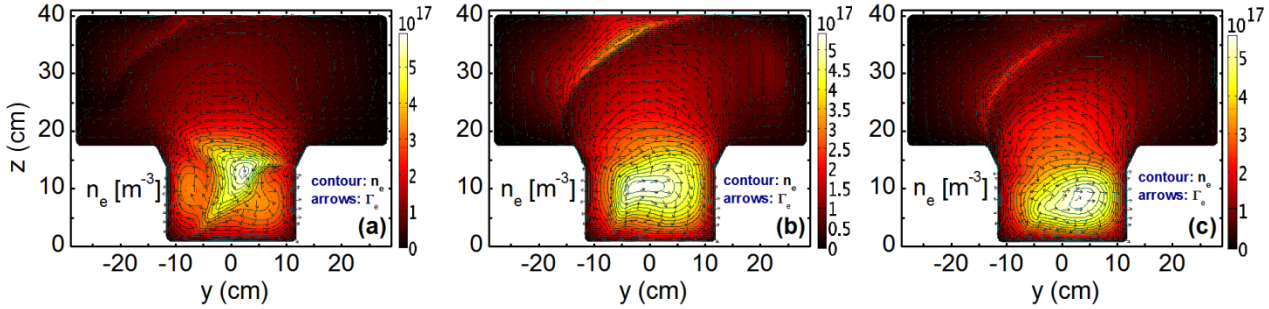

FIGURE 8. The same as in Fig. 7 but for the electron density.

The presence of a magnetic field in the driver has a local impact on the electron temperature (Fig. 7 compared to Fig. 5). In addition to the groove in the electron temperate in the expansion chamber, a second one is formed in the central region of the driver. Although the values of the magnetic field in the driver are low (roughly about 10 G) the thermal conductivity is enough suppressed to cause the formation of the latter.

The changes of the spatial distribution of the electron temperature, caused by the magnetic field in the driver, affect the spatial distribution of the electron density. The stronger asymmetry of the electron density profile in the driver (Fig. 8 compared with Fig. 6) results from mutual acting diffusion (suppressed by the magnetic field) and thermal diffusion (triggered by the temperature gradient) in the region of the second groove of the electron temperature. In complete analogy with the previous case (without FF inside the driver), the patterns of the electron temperature and of the electron density shift in correlation with the axial position of the MF.

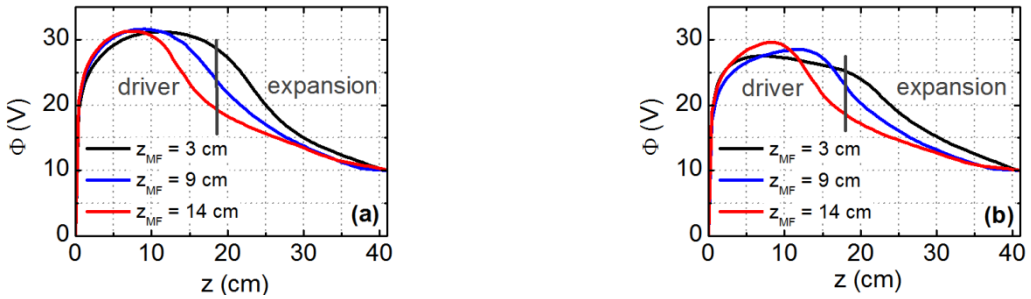

FIGURE 9. Axial variations of the plasma potential for different z_{MF}: (a) without and (b) with account for the FF in the driver.

Based on the comparison of the results shown in Figs. 5-8, it could be concluded that the presence of a magnetic field in the driver affects the electron temperature and the electron density locally, showing no significant influence

on their spatial distributions in the expansion chamber. However, the well pronounced asymmetry of the electron density in the driver, indicated also in experiments carried at the BATMAN test bed [2,9], may have a strong impact on the RF power deposition. The latter can be identified only by introducing of an electrodynamics (for describing the RF power deposition by the coil) in the initial set of equations (1-4).

In the presence of a transverse magnetic field, due to the reduced electron losses, caused by the suppressed transport coefficients, the electron temperature and, thus, the plasma potential have lower values. This is also the case here, where the PG is at a fixed potential and the position of the MF is varied. However, as it is shown in Fig. 9, the position of the filter affects the plasma potential mainly in the transition region between the driver and the second chamber. With the shift of the MF towards the PG the potential difference between the PG and the exit of the driver increases.

Magnetic Field Configuration Corresponding to the ELISE Source

Figure 10 shows the spatial distributions of the parameters in the RF prototype source obtained for an ELISE-like magnetic field configuration (Fig. 1(b)), which is planned to be investigated at BATMAN upgrade [11]. The plasma grid is biased at U_{PG} = 10 V, the RF power deposition is localized at the walls of the driver and the losses along the magnetic field are introduced. The patterns of the electron temperature (Fig. 10(a)) and the electron density (Fig. 10(b)) have all the main features as those obtained for the magnetic field configurations of the BATMAN test bed: groove of the electron temperature and second maximum of the electron density in the expansion chamber of the source. However, due to the low value of the magnetic field (20 G), they are less pronounced. The values of the magnetic field in the driver are also low, but the asymmetry in the spatial distribution of the plasma parameter is evident (even for the plasma potential in Fig. 10(c)).

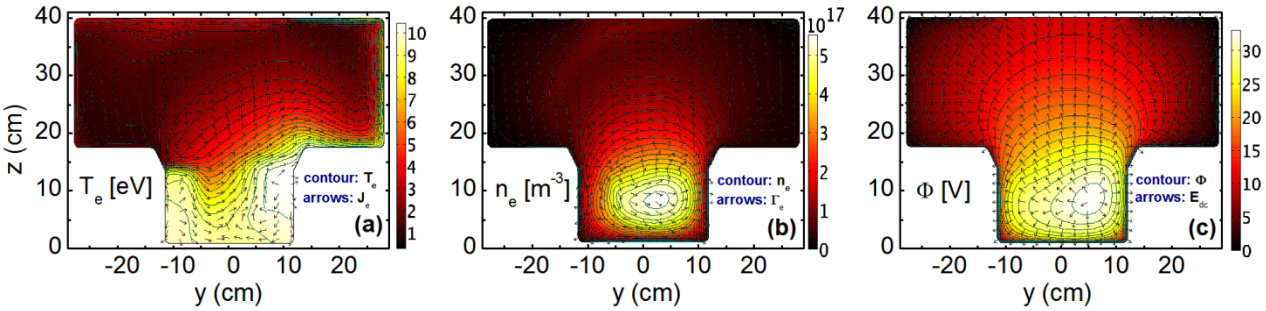

FIGURE 10. Spatial distribution of the electron temperature (a), of the electron density (b) and of the plasma potential (c) obtained for the magnetic field configuration of the ELISE (Fig. 2(b), B_{max} = 20 G). P_W = 40 kW; p = 0.6 Pa and U_{PG} = 10 V.

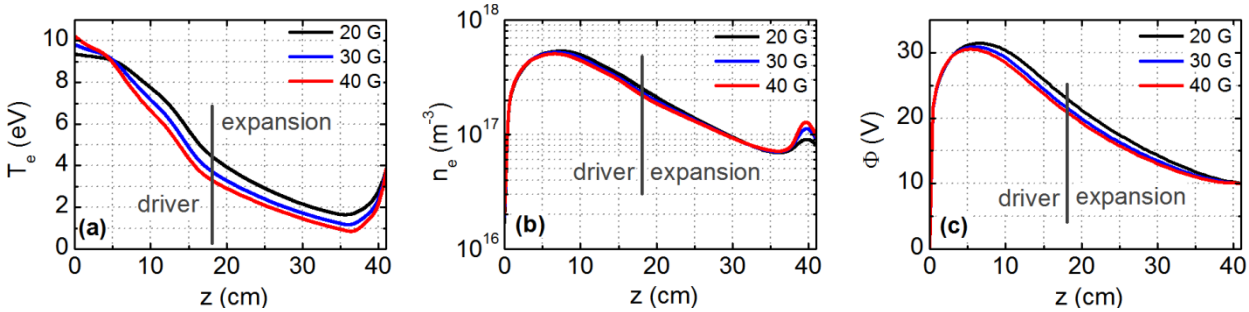

FIGURE 11. Axial variations (i.e., a cross-section at y = 0 cm) of the electron temperature (a), of the electron density (b) and of the plasma potential (c) obtained at different magnitudes of the magnetic field configuration of the ELISE. The same discharge conditions as in Fig. 10.

In contrast to the assumed magnetic field configuration of the BATMAN, where the axial position of the magnetic filter determines its configuration, here, the magnitude of the magnetic field can be varied. As it is shown in Fig. 11, the magnitude of the FF does not introduce significant changes in the axial profiles of the plasma parameters. The pattern of the plasma parameters is kept the same, which could be associated to the same spatial structure of the MF (Fig. 1(b)). However, increasing the FF causes a decrease of the electron temperature

(Fig. 11(a)) and of the plasma potential (Fig. 11(c)) as well as a local increase of the electron density just in front of the plasma grid (were the magnetic field has its maximum value).

CONCLUSIONS

In the study are presented numerical results showing the influence of the configurations of the magnetic fields of the BATMAN test bed and the ELISE source on the plasma parameters in the IPP RF negative ion source prototype for ITER. A previously developed 2D fluid plasma model of hydrogen discharge at low gas pressure has been used and extended towards accounting for the losses of particles and energy due to the third dimension (along the magnetic field) and the presence of a magnetic field in the driver.

Based on comparisons with results from a 3D model, it is shown that the simplified manner of accounting for the losses of particles and energy in the 2D model could be considered as a good approximation of the 3D case. The losses along the magnetic field do not introduce changes in the pattern of the plasma parameters (a groove in the spatial distribution of the electron temperature and a maximum of the electron density in the second chamber). However, due to the suppression of the drifts by the additional fluxes along the magnetic field lines, the structuring of the plasma parameter in the expansion chamber is less pronounced.

It is shown that for the magnetic field configuration of the BATMAN test facility, the presence of a magnetic filter in the driver (of about 10 G) affects the electron temperature and the electron density locally, causing a strong asymmetry of their profiles, and has no significant influence in the expansion chamber

Employing the magnetic field configuration of the ELISE into the prototype source geometry shows the same main features in the patterns of the electron temperature and the electron density as for the magnetic field configurations of the BATMAN test facility. It has been shown that the magnitude of the magnetic field does not introduce significant changes in the axial profiles of the plasma parameters.

Since the presence of a magnetic field in the driver may cause an asymmetry in the power deposition, introducing of an electrodynamics in the model (for describing of the RF power deposition by the coil) should be the next step in the extension of the model, performed together with comparison with the recent experimental result carried out at the BATMAN test bed. Such basic studies are useful also in a view of optimization and improvement of the future sources developed towards DEMO (e.g., in the replacement of two cylindrical driver with one race-track driver [11]).

ACKNOWLEDGMENTS

This work has been carried out within the framework of the EUROfusion Consortium and has received funding from the European Union's Horizon 2020 research and innovation programme under grant agreement number 633053. The views and opinions expressed herein do not necessary reflect those of the European Commission.

REFERENCES

1. P Franzen at al., Plasma Phys. Cont. Fusion **53**, 115006 (2011)
2. M. Fröschle et al, Fusion Engineering and Design **88**, 1015–1019 (2013).
3. U. Fantz et al, Nucl. Fusion **49**, 125007 (2009).
4. L. Schiesko, P. McNeely, P. Franzen, U. Fantz and the NNBI Team, Plasma Phys. Control. Fusion **54**, 105002 (2012).
5. St. Kolev, St. Lishev, Kh. Tarnev, A. Shivarova and R. Wilhelm, Plasma Phys. Control. Fusion **49**, 1349 (2007).
6. G. J. M. Hagelaar and N. Oudini, Plasma Phys. Control. Fusion **53**, 124032 (2011).
7. G. Fubiani et al, Phys. Plasmas **19**, 43506 (2012).
8. S. Lishev, L. Schiesko, D. Wünderlich and U. Fantz, (NIBS 2014, October 6-10, 2014, IPP Garching, Germany) in: AIP Conf. Proc., **1655**, 040010 (2015).
9. U. Fantz, L. Schiesko and D. Wünderlich, Plasma Sources Sci, Thechnol. **12**, 044002 (2014.)
10. R. Hemsworth et al, Nucl. Fusion **49**, 045006 (2009).
11. B. Heinemann et al, (NIBS 2014, October 6-10, 2014, IPP Garching, Germany) in: AIP Conf. Proc., **1655**, 060003 (2015).
12. St. Lishev, A. Shivarova and Kh. Tarnev, J. Plasma Phys., **77**, No. 4, pp. 469-478 (2011).